A facile way to synthesize noble metal free TiO_2 based catalysts for glycerol photoreforming

Claudio M. Pecoraro, Marianna Bellardita*, Vittorio Loddo, Francesco Di Franco, Leonardo Palmisano, Monica Santamaria

Dipartimento di Ingegneria, Università degli Studi di Palermo, Viale delle Scienze Edificio 6, 90128 Palermo, Italy

Corresponding autor: Marianna Bellardita, E-mail: marianna.bellardita@unipa.it

Abstract

In this work anaerobic heterogeneous photocatalytic solar/UV light reforming of glycerol in aqueous media was performed with Pt-photodeposition and noble metal free modified TiO_2 photocatalysts prepared through ball milling, a very simple and cheap coupled catalyst preparation method. Different amounts of Cu_2O or 3% CuO were loaded on TiO_2 using ball milling and during each run glycerol conversion, hydrogen and CO_2 formed in the gas phase and 1,3-dihydroxyacetone (DHA) and glyceraldehyde (GA) in the liquid phase were determined. The results were compared with the aim to verify the effectiveness of Cu_2O in replacing Pt. Using noble metal free photocatalysts, 33% glycerol conversion, 10.3% and 5.4% selectivity towards DHA and GA, respectively, a CO_2 concentration of 0.16 mM, and a H_2 concentration of 1.01 mM corresponding to 0.17 mmol h^{-1} g^{-1} were obtained. Ex situ photoelectrochemical characterization confirmed the formation of a heterostructure between TiO_2 and copper oxide and the effectiveness of Cu_2O towards H_2 formation.

Keywords: Photocatalytic glycerol partial oxidation, High added value chemicals, Ball milling heterostructure formation, H_2 production, TiO_2

1. Introduction

In the last years, with the growing energy demand and the related CO_2 emissions, a lot of efforts toward renewable, low carbon sources have been made [1].

By considering the various opportunities, the cheapest, most abundant and easily usable energy is the solar one, and it could be deployed for an environmentally friendly, sustainable and low-carbon emission industry [2]. Heterogeneous photo-catalysis has been studied in many applications in the last few years, like organic synthesis [3,4], decomposition of pollutants [5,6], water splitting [7,8] and photo reforming [9,10].

Recently, from this point of view, a valid way forward has been the exploitation of glycerol, a biomass derivative obtained in large quantities as a waste product of the biodiesel production industry.

Recently, from this point of view, a valid way forward has been the valorization of glycerol, a biomass derivative obtained in large quantities as a waste product of the biodiesel production industry [1,11]. In addition, glycerol, compared to other biomass components, has gained great attention due to its ease of hydrogen formation [12].

Regarding the photocatalysts studied for glycerol reforming, TiO_2 has aroused great interest as an anodic site for substrate oxidation because it is an abundant, cheap and non-toxic material, which shows good thermal- and photo-stability [13]. As cathodic site, responsible for H_2 evolution, a noble metal like platinum has been often used [14–16] and today few cheap alternatives with activities comparable to noble metals can be found in literature [17–21]. Mandari et al. synthetized onto the surface of titania particles CuO and $Cu_3(PO_4)_2$ clusters as promising photo-catalyst for the production of high quantities of H_2 from glycerol-water solutions [22]. Gultom et al. obtained a hydrogen production rate up to14800 μmol $g^{-1}h^{-1}$ using a Ni doped ZnO-ZnS solid solution (Zn(O,S)) in 50% ethanol-water mixture [23]. The use of Cu_2O is particular interesting because it presents different advantages as low toxicity, low cost, low band gap (2.0-2.2 eV) and conduction band energy suitable for H^+ reduction [23]. The major drawback of this oxide is the instability of Cu^+ in the presence of humidity and light; one possible approach to improve its stability is to slow down the charge recombination by coupling it with other semiconductors [23–25].

This manuscript reports the results of anaerobic heterogeneous photocatalytic solar/UV light glycerol reforming in aqueous solution, using commercial TiO_2 loaded with platinum and/or coupled with copper oxide in order to verify the efficacy of Cu_2O in replacing Pt for the formation of hydrogen. The coupled samples were obtained by a simple and inexpensive

ball grinding approach that allowed for the easy preparation of large quantities of catalyst in view of the use of pilot plant scale reactors [27].

In each experiment the quantity of hydrogen and CO_2 formed in the gas phase and that of DHA and GA in the liquid phase resulting from the partial oxidation of glycerol were monitored [28]. The latter compounds are considered valuable chemicals, in particular DHA is used in the cosmetic industry and as a monomer for the production of polymeric biomaterials, while GA is an intermediate used in the preparation of polyesters and adhesives and as a cellulose modifier.

2. Experimental section

2.1. Samples preparation

P25 (TiO_2 P25 Degussa), $PtCl_4$ (BDH Chemicals) Cu_2O (Riedel-de Haën), CuO (Sigma Aldrich), glycerol (Sigma Aldrich), 1,3-dihydroxyacetone (Sigma Aldrich), glyceraldehyde (Sigma Aldrich), ammonium biborate tetrahydrate (ABE, $(NH_4)_2B_4O_7{\cdot}4H_2O$; Sigma Aldrich), propylene carbonate (Sigma Aldrich), were used as received.

The photocatalysts were prepared in a simple way. 3% wt CuO, 2% - 4% wt Cu_2O, and 3% wt (Pt Cu_2O) were mixed with commercial TiO_2 P25 by using a Retsch Ball Mills, type PM100. For each preparation the solid components were mixed 2 hours, at 150 rpm, reversing the sense of the rotation after 1 hour and 10 minutes of pause. 0.5% wt of Pt was loaded on Cu_2O and 3%Cu_2O TiO_2 by a photo deposition method as follows: 400 mL of H_2O, 2 g of TiO_2, 50 mL of ethanol, and 0.02 g of $PtCl_4$ were added to an 800 mL photoreactor. Nitrogen was bubbled for 30 minutes in the dark to remove the oxygen and during the irradiation of the dispersion (about 7 h with UV light) which allowed the photo-deposition of Pt. Subsequently the dispersion was evaporated to approx. 353 K to obtain the solid photocatalysts.

2.2. Samples characterization

XRD (X-Ray diffraction) patterns of the different photocatalysts were acquired by means of a PANalytical Empyrean diffractometer at room temperature. The PIXcel1D (tm) detector worked under a current of 40 mA and a voltage of 40 kV by using the CuKα emission tube. The 2θ investigated scan range was set from 20 to 60° with a scan rate of 3°/min.

Raman spectra were recorded by a Raman Microscope coupled with a Leica DMLM microscope. The laser was focused on the sample by a 5x magnification lens in order to obtain an analyzing spot diameter around 50 microns, with a maximum power of 133mW on the sample. Only the 10% of maximum power has been used in these measurements, the power was reduced by holographic filters, three for each sample, and the spectra have been recorded using a 532nm laser coupled with a 2400 lines per millimeter grating resulting in a spectral resolution equal to 0.5cm^{-1}. Each measurement consists of two accumulations.

A Shimadzu UV-2401 PC spectrophotometer was utilized to record the Diffuse Reflection Spectra (DRS) in the 200–800 nm region at ambient conditions and by using $BaSO_4$ as a reference.

The specific surface areas (SSA) of the samples were evaluated by a Micromeritics Flow Sorb 2300 instrument by employing the single-point (Brunauer–Emmett–Teller) BET method.

The SEM (Scanning electron microscopy) images were taken by mean of a FEI Quanta 200 ESEM microscope operated at an accelerating voltage of 30 kV. The elementary composition of the samples was investigated by an electron microprobe used in an energy dispersive mode (EDX).

The photoelectrochemical characterization was carried out using a UV-VIS Xenon lamp (power 450 W), whose light was sent to a monochromator in order to allow the irradiation of the sample surface by a selected wavelength through the quartz window of the cell. The electrode potential was controlled by a potentiostat and the measured current was sent to a two phase lock-in amplifier to isolate the photocurrent from the overall current circulating in the cell. A mechanical chopper was used to stop the irradiation at a known frequency (namely 13 Hz).

For the photoelectrochemical measurements P25, 3%CuO-P25 and 3%Cu_2O-P25 photocatalysts were drop casted on carbon paper support (Toray 40% wet Proofed-E-Tek) and immersed in 0.1 M ammonium pentaborate (ABE) aqueous solution (pH ≈ 9) in a three-electrode configuration cell. A Pt wire was used as counter electrode, and a silver/silver chloride (Ag/AgCl/sat. KCl) was employed as reference electrode (0 V vs Ag/AgCl = 0.197 V vs SHE).

The EPR spectra for the investigated photocatalysts were collected at room temperature in dark or upon continuous in situ photoexcitation by UV light (maximum wavelength 365 nm; Bluepoint LED, Hönle UV Technology). An EMX EPR spectrometer purchased from Bruker was used for this purpose. The latter operates in X-band at 100 kHz field modulation in the

standard TE102 (ER 4102 ST) rectangular cavity using EPR tubes made in quartz with thin walls (Bruker).

2.3. Photocatalytic tests

The photocatalytic activity of the used catalysts was studied in a 250 mL cylinder-shaped Pyrex reactor by using a 125 W medium pressure Hg lamp (main emission peak at ca. 365 nm) or a 150 W halogen lamp (simulating the solar spectrum) as irradiation sources. The catalysts were added to the glycerol solution and Helium was gurgled in the dispersion under stirring in the dark for the time necessary for the substrate to reach saturation of the surface of the catalysts (0.5 h), then the reactor was closed, and the lamp switched on. The runs were carried out at ca. 303 K by circulating water in the reactor jacket with an initial glycerol concentration of 2 mM and 0.3 g/L of catalyst (determined by light absorption tests [26]). The tests were performed twice and the results obtained differed by ca. 2%. To follow the concentration of the species in the reaction mixture, aliquots of the dispersion were withdrawn at fixed times, filtered by using a 0.2 µm PTFE filter and analyzed by a HPLC instrument (Thermo Scientific Dionex UltiMate 3000) equipped with a REZEK ROA Organic acid H^+ column. The eluent consisted of a $2.5 \cdot 10^{-3}$ M H_2SO_4 solution with a flow rate of 0.6 mL min^{-1}.

CO_2 and H_2 accumulated in the head space gaseous phase were collected by a gas-tight syringe and quantified by a TCD (thermal conductivity detector) installed on a gas chromatograph HP 6890. The compounds were separated by a packed 60/80 Supelco GC column.

3. Results and discussion

Figure 1 shows X-ray diffraction patterns of TiO_2 P25 (referred to simply as P25 in the following), 2% Cu_2O P25, 3% Cu_2O P25, 4% Cu_2O P25, 3% (Pt Cu_2O) P25, Pt-(3%Cu_2O P25) and 3% CuO P25. In the sample 3% (Pt Cu_2O) P25 the platinum was added by the photodeposition method described in the experimental section only to commercial Cu_2O and then mixed to P25 through balls milling, while in the sample Pt-(3%Cu_2O P25) it was added using the same method to 3% Cu_2O P25 previously prepared through balls milling.

Figure 1 a) and b) show, respectively, X-ray diffraction patterns within 2θ range 20°-50° and 50°-90°, where the peaks relative to the two phases of TiO_2 anatase (A) and rutile (R),

characteristic of the commercial P25, have been identified [27]. A close inspection of the 2θ=25.3° peak of anatase (Figure 1b) reveals a slight shift to lower angles for the sample Pt-(3%Cu_2O P25). For TiO_2 samples doped with metal species having an ionic radius similar to that of the Ti^{4+}, the shift was attributed to the reticular deformation resulting from the insertion of the metal ion in a substitutional position [28,29]. In our case, this shift can be due to the interaction of Pt with Cu^+ in accordance with Wang and Wang who observed some degree of photocorrosion of Cu_2O in the presence of Pt [30].

Magnifications of 2θ range between 35° and 40° are shown for all the samples in Figure 1 d). Figure 1 e) shows X-ray diffraction patterns of P25 and 3% CuO P25. While P25 pattern shows peaks related to A and R TiO_2 phases, a small peak related to crystalline CuO can be identified in the 3% CuO P25 pattern, despite the low concentration of CuO in the mixture [31]. A similar behaviour can be seen in Figure 1 f) where a small peak related to Cu_2O can be identified [32].

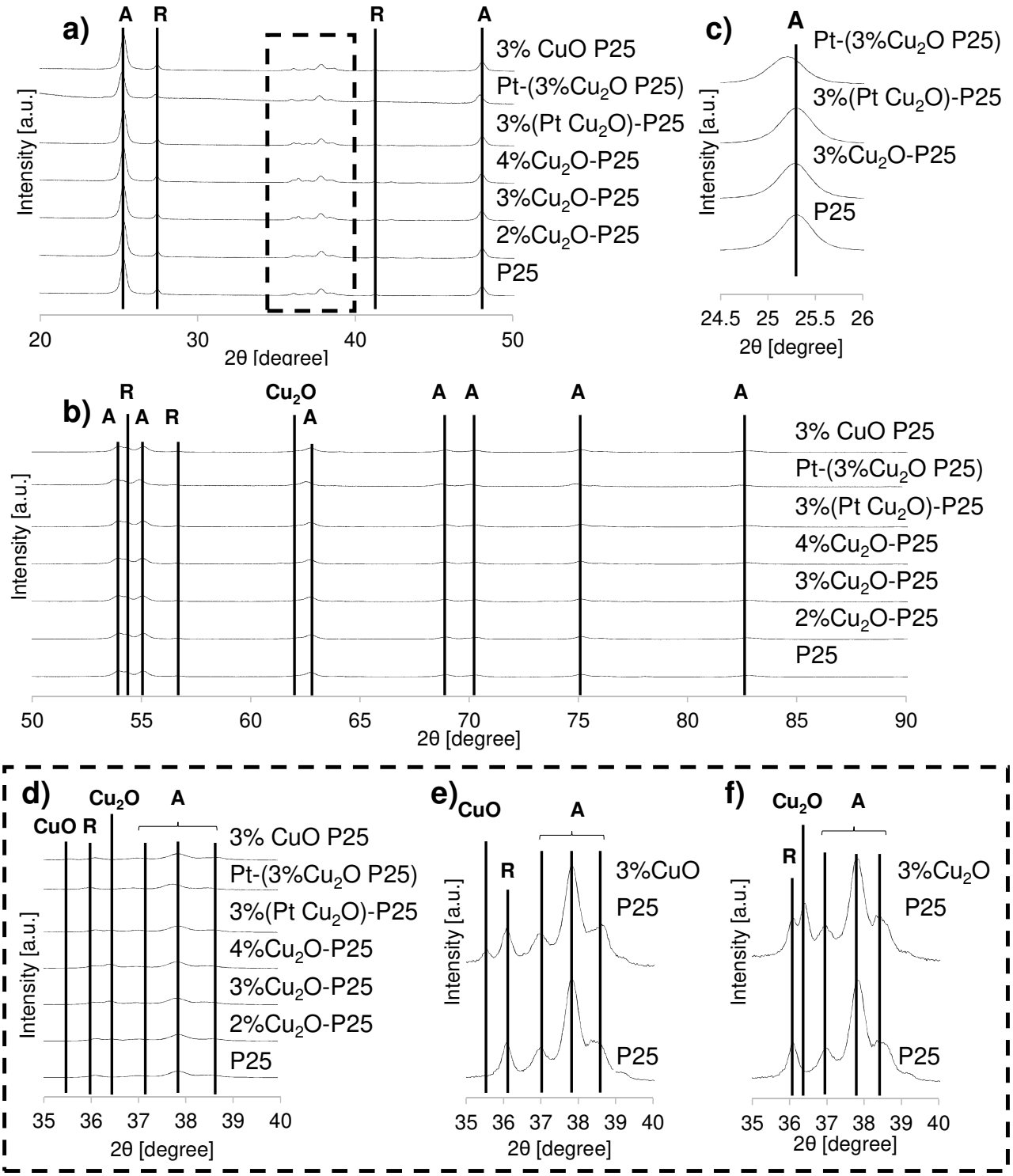

Figure 1. X-ray diffraction patterns of P25, 2% Cu_2O P25, 3% Cu_2O P25, 4% Cu_2O P25, 3% (Pt Cu_2O) P25, Pt-(3%Cu_2O P25) and 3% CuO P25 within 2θ range of a) 20°-50°, b) 50°-90° and d) 35°-40°. Magnifications of P25, 3% Cu_2O P25, 3% (Pt Cu_2O) P25 and Pt-(3%Cu_2O P25) within 2θ range of 24.5°-26° is shown in c), while P25 and 3% CuO P25 or 3% Cu_2O P25 within 2θ range of 35°-40° are shown respectively in e) and f). The peaks A and R are related respectively to the anatase and rutile phase of TiO_2, CuO and Cu_2O to the respective copper oxide.

In Figure 2, the Raman spectra of modified samples and pure Cu_2O and CuO are reported.

The characteristic bands of anatase at 144 cm^{-1}, 196 cm^{-1}, 397 cm^{-1}, 513 cm^{-1}, and 639 cm^{-1} are indicated [33]. No signals related to Cu_2O, CuO or Pt can be observed, due to their low amount and good dispersion on TiO_2 surface. The enlargement of main anatase band at 144 cm^{-1}, see inset, reveals a little shift towards higher wave numbers for the samples 3% Cu_2O P25 and Pt-(3% Cu_2O P25) attributable to the interaction between the two oxides.

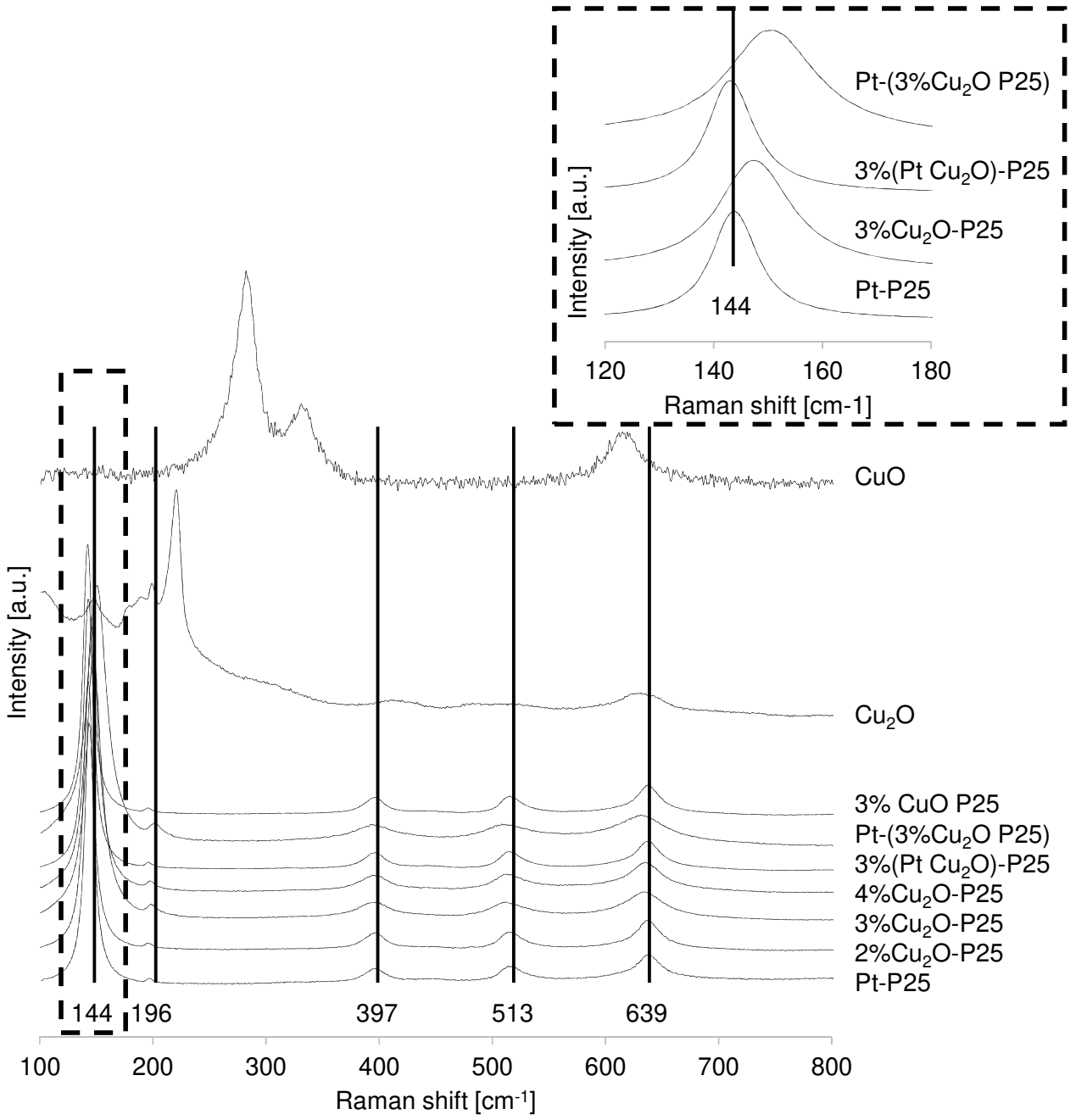

Figure 2. Raman spectra of tested samples and pure CuO and Cu_2O. Enlargement of main anatase band at 144 cm^{-1} is shown in the inset

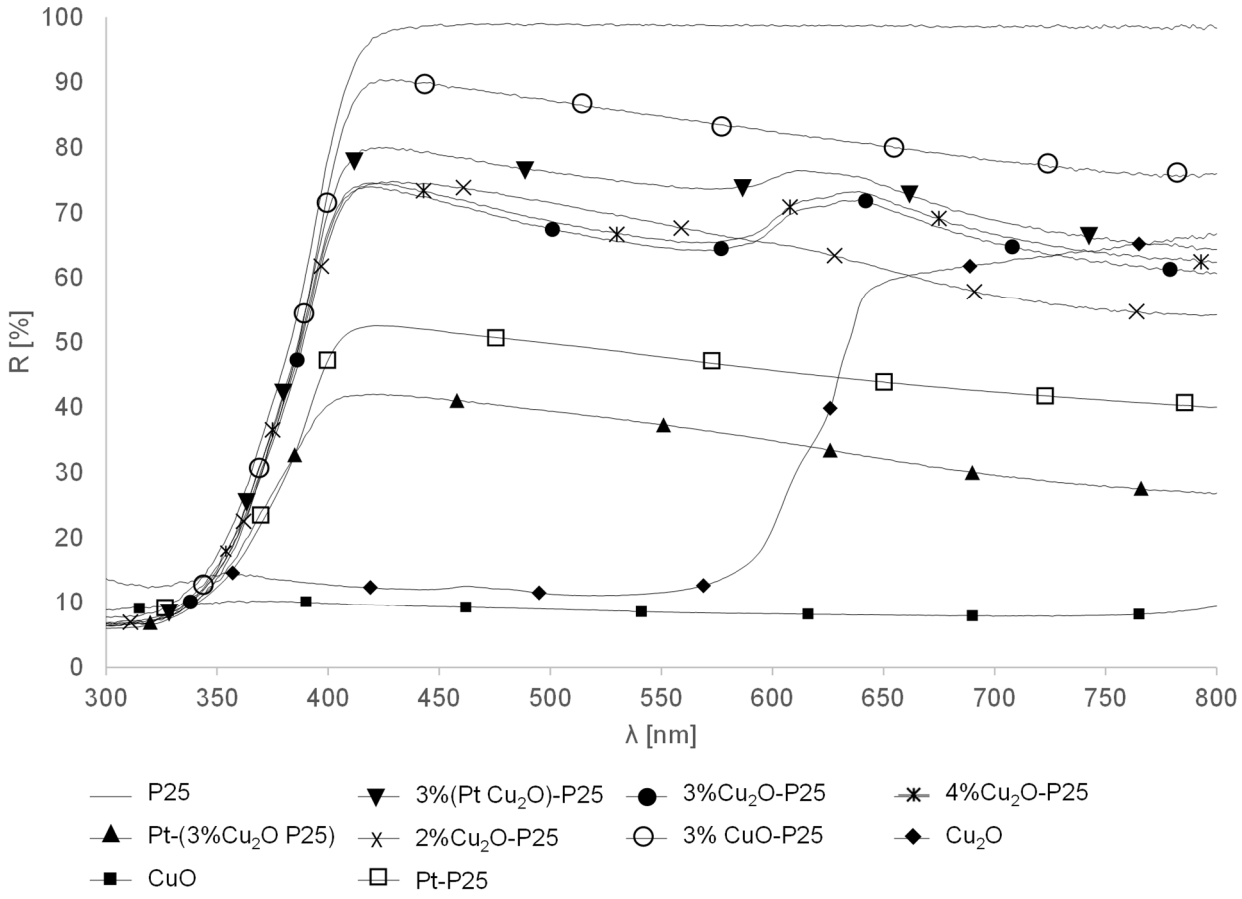

Figure 3. DRS spectra of the various samples

Figure 3 shows the diffuse reflectance spectra of all of the investigated powders. The commercial P25 shows an onset in absorption at ca. 360 nm corresponding to the typical band-gap of anatase, since rutile is in smaller quantities than anatase.

In the samples 2%-4% Cu_2O P25 can be noticed a small shift in the absorption to higher wavelengths, < 610 nm, and the shift is higher for 3% Cu_2O P25 and 4% Cu_2O P25. In the samples containing Pt a decrease in the reflectance can be noticed without any change in the absorption edges.

From the reflectance data the band gap values (E_g) were calculated by drawing the tangent lines to the graph of the modified Kubelka-Munk function, $[F(R'_\infty)hv]^{1/2}$, versus the energy of the exciting light. The obtained values are reported in Table 1. Commercial P25 displays a band-gap values of 3.14 eV typical of the anatase-rutile mixture; the deposition of Pt does not modify the value but increases the absorption in the visible region (Figure 3). The band gap of commercial Cu_2O is 1.99 eV, in accordance with the literature [25,34] whilst it was not possible to measure the value for CuO due to the high absorption over all the measured wavelengths range (Figure 3). The composites samples containing Cu_2O present two

absorption edges corresponding to the two oxides (at ca. 3.10 eV for TiO_2 and ca. 2.00 eV for Cu_2O) that confirm the formation of a heterostructure [26,35]. In samples with the presence also of Pt or CuO, it is possible to calculate only the band bap corresponding to TiO_2 in accordance with the reflectance spectra reported in Figure 3.

Table 1 Band-gap (Eg) and Specific Surface Area (S.S.A.) values of the different samples.

Sample	E_g (eV)	S.S.A. ($m^2 g^{-1}$)
P25	3.14	50
Pt-P25	3.12	48
Cu_2O	1.99	1
2% Cu_2O P25	3.08 2.02	51
3% Cu_2O P25	3.10 2.00	48
4% Cu_2O P25	3.09 2.00	48
Pt-(3%Cu_2O P25)	3.20	48
3% (Pt Cu_2O) P25	3.06	48
3% CuO P25	3.06	47

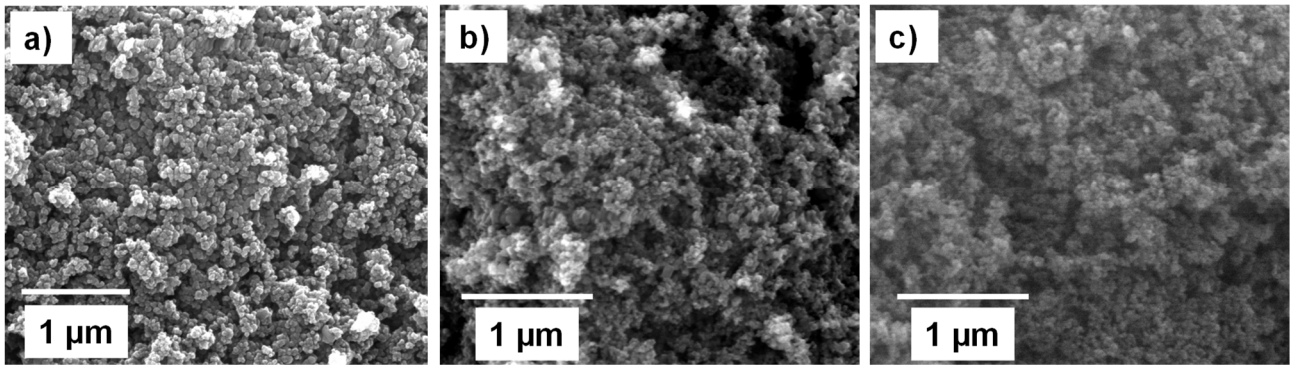

Figure 4. SEM images of a) Pt-P25 (without ball milling treatment), b) 3% Cu_2O P25, c) Pt-(3%Cu_2O P25).

Figure 4 shows the SEM image of Pt-P25 (Figure 4a), in which Pt was deposited on the as the received commercial catalyst, and the composite samples obtained by ball milling (Figure 4b and 4c).

All the samples are formed by aggregates of irregular spherical small particles, lower than 500 nm, confirming the high surface area of the powders. No substantial variations are observed when comparing Figures 4a and 4b indicating that the ball milling treatment did not induce any aggregation of particles, probably due to the mild experimental conditions (rotation speed = 150 rpm). Furthermore, the Cu_2O particles are not distinguishable, confirming their high degree of dispersion within the TiO_2 mass.

By the EDX analysis the presence of Cu and Pt was verified and their quantities are very similar to the nominal values, confirming the effectiveness of both balls milling and the photodeposition. Measurements carried out at different points gave approximately the same values highlighting the homogeneous distribution of the foreign species in the host material. TEM analyses performed in similar samples confirmed the formation of a heterojunction between TiO_2 and Cu_2O [21].

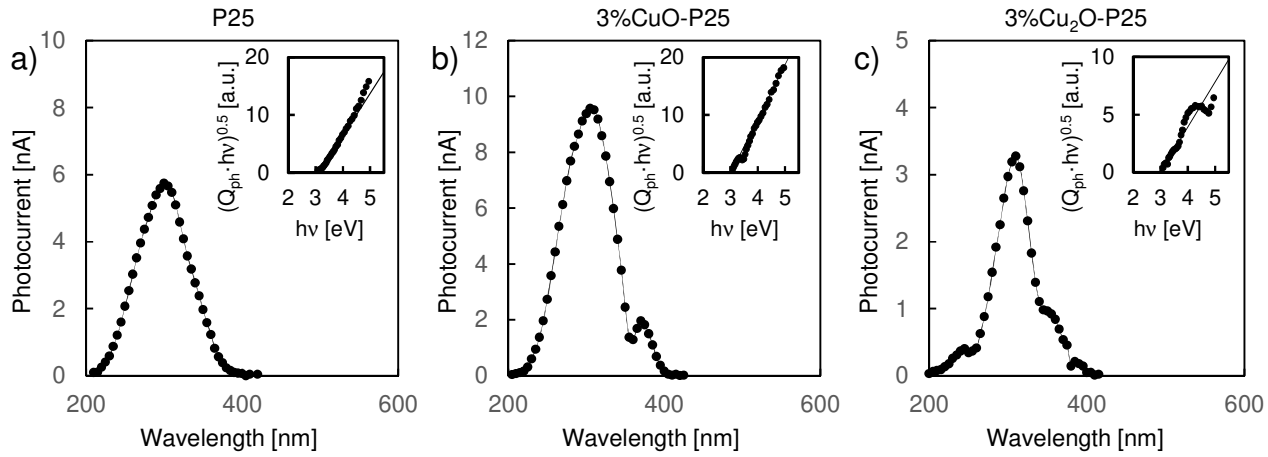

Figure 5. Photocurrent spectra for a) P25, b) 3%CuO-P25, c) 3%Cu_2O-P25, recorded in ABE 0.1 M solution (pH ~ 8) at UE ~ 0 V vs. Ag/AgCl. The insets show the respective $(Q_{ph}\ h\nu)^{0.5}$ vs hν plots.

Photoelectrochemical measurements were carried out with the aim to study the influence of copper oxide addition on the electronic properties of the photocatalysts. The photocurrent spectra recorded in 0.1 M ABE at the open circuit potential (U_E ~ 0 V vs. Ag/AgCl) are reported in Figure 5. Notably, for 3%Cu_2O P25 and 3%CuO P25, in the wavelength range between 350 nm and 400 nm a second photocurrent maximum is present indicating the presence of two electronic transitions. Under the hypothesis of non-direct optical transitions, the optical band gap (E_g) values of the investigated catalysts can be determined according to the following Equation 1:

Eqn. 1) $$(Q_{ph}\ h\nu)^{0.5} \propto (h\nu - E_g)$$

where hν is the photon energy and Q_{ph} is the photocurrent yield. The latter is defined as the measured photocurrent corrected for the efficiency of the lamp monochromator system, which in turn is proportional to the light absorption coefficient for hν values near the band gap. As disclosed in Figure 5 (see inset) the optical band gaps of all the photocatalysts are estimated by extrapolating to zero the $(Q_{ph}\ h\nu)^{0.5}$ vs hv plots. For P25 E_g of 3.15 eV was determined, while for 3%Cu_2O P25 and 3%CuO P25 a slightly lower band gap of 3.0 eV was estimated that can be attributed to the presence of copper oxide particles. Indeed, photocurrent at photon energy lower than the band gap of P25 is measured due to optical transitions, therefore the presence of copper oxides induces a redshift of the light absorption threshold in agreement with the experimental findings obtained by DRS. Moreover, these experimental results confirm that TiO_2/Cu_2O and TiO_2/CuO junctions are stable in aqueous solution.

In Table 2 the results of the photocatalytic runs are reported in terms of conversion of glycerol, amount of CO_2 and H_2 and selectivity towards the main oxidation products. All the runs were carried out at pH ≈ 7 (the natural pH obtained by adding the catalysts to the glycerol aqueous solution). As far as the Pt-P25 is concerned, the natural pH (pH=3.5) was adjusted to 7 by a solution of NaOH.

The main glycerol partial oxidation products identified in the aqueous phase were 1,3-dihydroxyacetone and glyceraldehyde whilst CO_2 and H_2 were measured in the gas phase. In the presence of bare P25 no hydrogen formation was observed, then two different strategies have been used: the photodeposition of Pt, as it is the most active metal towards H_2 formation, and the coupling with Cu_2O, with the aim to replace the noble metal with a less expensive and dangerous species.

Pt-P25 was effective in the oxidation of glycerol with a conversion of 40.6 % after 5 h of irradiation and DHA selectivity of 11.4 %, and no GA was formed in the liquid phase. The maximum H_2 amount was 0.99 mM with an average production rate of 0.17 mmol $h^{-1}g^{-1}$. By considering the coupled systems, first the effect of the weight ratio between Cu_2O and P25 was studied. All the samples showed both a good oxidant activity and H_2 formation capability demonstrating that Cu_2O is an excellent substitute for Pt. By increasing the amount of Cu_2O from 2 to 4%, the activity first increased and then decreased, being 3% Cu_2O P25 the best sample. In the presence of this photocatalyst, approximately, the same amounts of CO_2 and H_2 as those obtained with Pt-P25 were produced with a glycerol conversion of ca. 33%. In the presence of Cu_2O also GA was formed due probably to the different surface properties

with respect to pristine P25. With the aim to increase the catalysts performance and investigate the role of cuprous oxide, other samples were studied. By coupling P25 with 3%Pt-Cu_2O a decrease in the photoactivity with respect to 3% Cu_2O P25 was observed probably due to the Cu^+ photocorrosion under irradiation when in close contact with Pt [30]. In the presence of the sample obtained after photodeposition of Pt onto the 3% Cu_2O P25 composite, the same photoactivity of this latter was obtained confirming that Pt Cu_2O plays the same role as Pt. On the contrary, by coupling CuO with P25 (3% CuO P25), a significant decrease in activity was obtained compared to 3% Cu_2O P25. This finding is ascribable to the position of the edge of the conduction band of CuO which, being less negative than that of TiO_2, is energetically less favorable than that of Cu_2O towards the production of H_2. The conduction band edge of CuO is, in fact, very near to the H^+/H_2 reduction potential [36,37]. On the contrary, the conduction band edge of Cu_2O is more negative than that of TiO_2 so that the photogenerated electrons are more effective to reduce H^+ to H_2 [24,38,39].

Table 2 Results obtained after 5 h of UV irradiation. X = glycerol conversion, S = selectivity. DHA = 1,3-dihydroxyacetone, GA = glyceraldehyde

Sample	X [%]	S_{DHA} [%]	S_{GA} [%]	CO_2 [mM]	H_2 [mM]	H_2 [$mmolh^{-1}g^{-1}$]
Pt-P25	40.6	11.4	-	0.15	0.99	0.17
2% Cu_2O P25	22.3	9.55	13.5	0.08	0.35	0.06
3% Cu_2O P25	32.9	10.3	5.39	0.16	1.01	0.17
4% Cu_2O P25	21.3	9.94	11.2	0.08	0.45	0.07
3%(Pt Cu_2O) P25	27.5	8.23	7.9	0.10	0.58	0.09
Pt (3% Cu_2O P25)	35.2	9.19	7.89	0.19	1.10	0.18
3% CuO P25	11.5	16.1	11.2	0.05	0.33	0.05
3% Cu_2O P25*	-	-	-	-	0.04	0.007

Figure 6 a) shows the concentration vs. time of glycerol and its products for the run carried out in the presence of the sample 3% Cu_2O P25. During the reaction time glycerol decreased and CO_2 increased, while DHA, GA and H_2 reached asymptotic values.

In Figure 6 b) curve of H_2 production versus reaction time shows a peak of 0.37 mmol h^{-1} g^{-1} after one hour and a decrease to 0.17 mmol h^{-1} g^{-1} after five hours of reaction time because of the asymptotic H_2 concentration and the increasing reaction time. This can be probably

due to the contemporary formation of little amount of O_2 deriving from water splitting. The competition of oxygen with H^+ for electrons and the occurrence of the back reaction between H_2 and O_2 decrease the H_2 evolution rate [15]. To verify the stability of the 3% Cu_2O P25 photocatalyst, it was recovered from the reaction mixture at the end of the run and reused. A good photostability was observed, but a decrease of ca. 10% in the H_2 formation was noticed, ascribable to a reduction of a little percentage of Cu^+ into metallic copper [21].

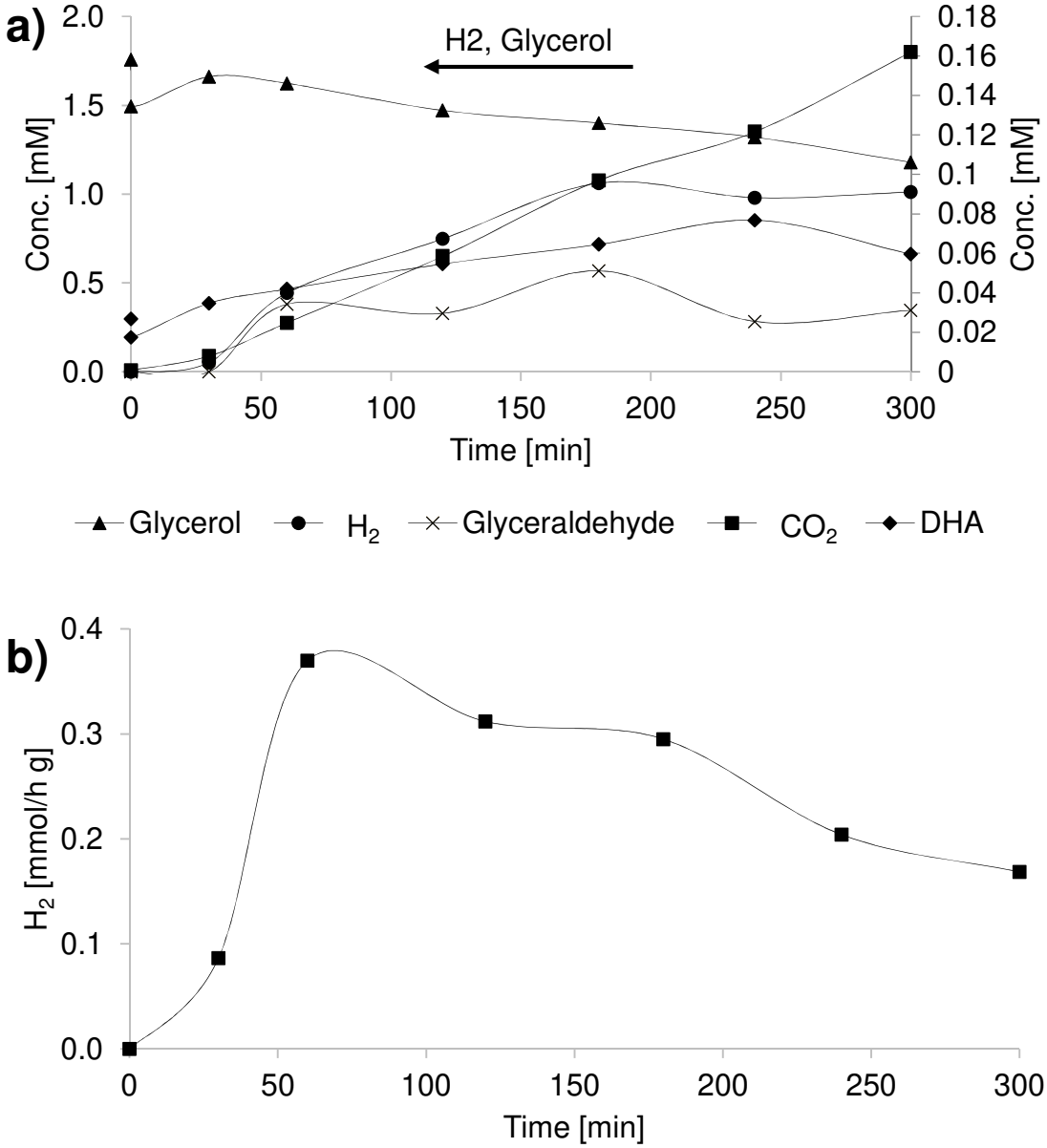

Figure 6. a) Concentration vs. time and b) H_2 production versus reaction time with the samples 3% Cu_2O P25.

A run was performed with the 3% Cu_2O P25 sample in pure water. A low quantity of hydrogen was obtained by water splitting, confirming the positive effect of a sacrificial agent on the production of H_2 with the further advantage of using the holes for the formation of

valuable compounds deriving from the partial oxidation of glycerol. No hydrogen was obtained by using Pt P25 under the same experimental conditions

The photoactivity of the Pt P25 and 3% Cu_2O P25 samples was compared also under simulated solar light irradiation (Figure 7). Even in this case cuprous oxide had a beneficial effect both towards the partial oxidation compounds and H_2 formation. This finding is interesting in the view of utilization of these catalysts in a pilot plant reactor under direct solar light irradiation.

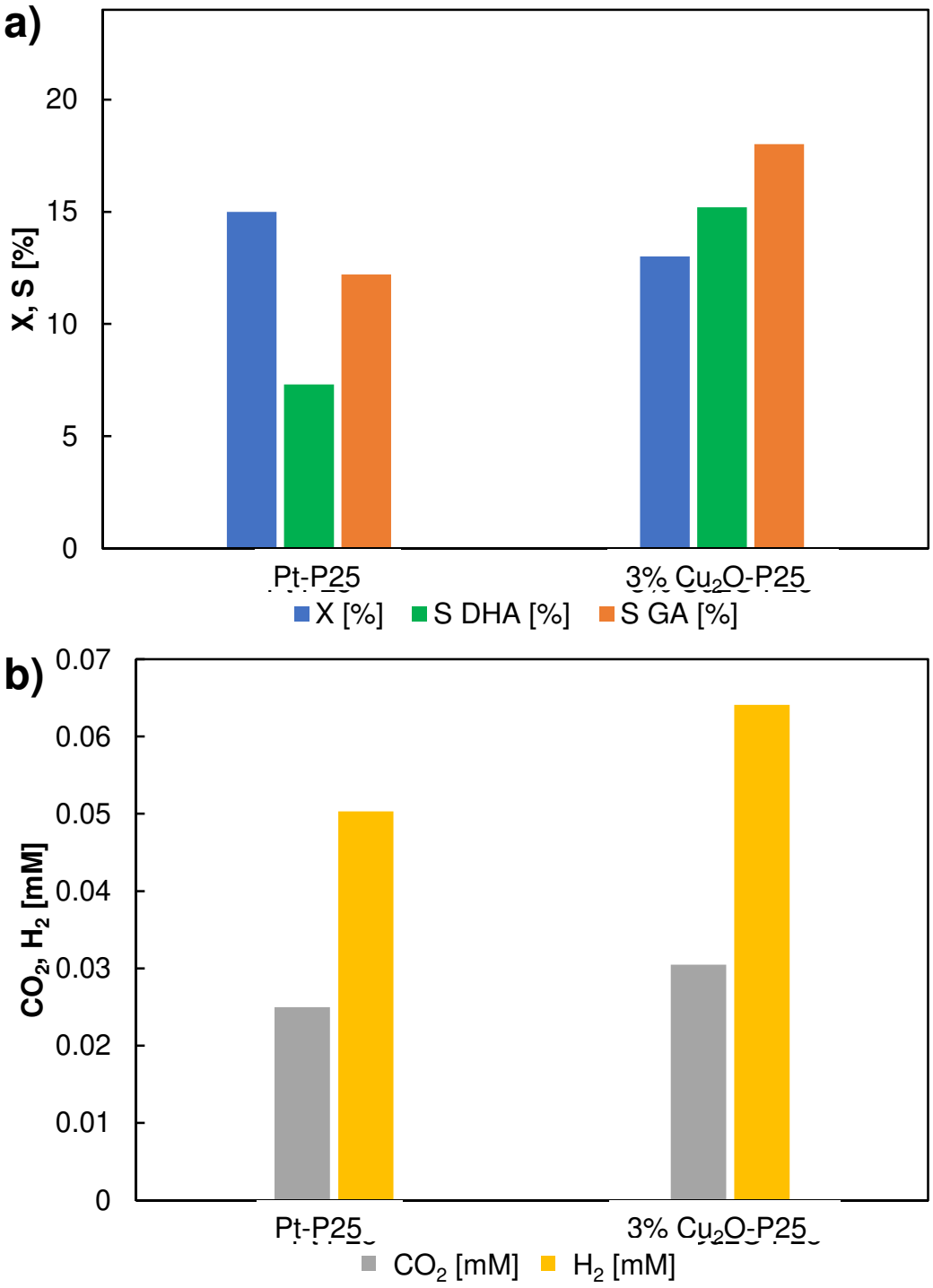

Figure 7. Values of a) conversion (X), selectivity towards 1-3 dihydroxyacetone (S DHA), selectivity towards glyceraldehyde (S GA) and b) CO_2 and H_2 concentrations of runs carried out in the presence of Pt-P25 and 3% Cu_2O-P25 using 150w halogen lamp.

By coupling Cu_2O with TiO_2 a p-n heterojunction is generally formed. Under UV light irradiation both oxides are excited and, by considering the bands edge position (Figure 8) [23,24,38], electrons are transferred from the conduction band of Cu_2O to that of TiO_2 and

holes from the valence band of TiO_2 to that of Cu_2O, enhancing the charges separation and increasing their lifetime. For this system also the formation of a direct Z-scheme has been reported [38,40,41] (Figure 7 green path). After irradiation, the TiO_2 conduction band's electrons recombines with the Cu_2O valence band's holes and electrons with high reduction ability and holes with high oxidation power are available. The negative potential value of the Cu_2O conduction band edge could explain the high activity of Cu_2O P25 samples with respect both to Pt-P25 and CuO P25. Moreover, the Z-scheme mechanism avoids the photocorrosion of Cu_2O [42].

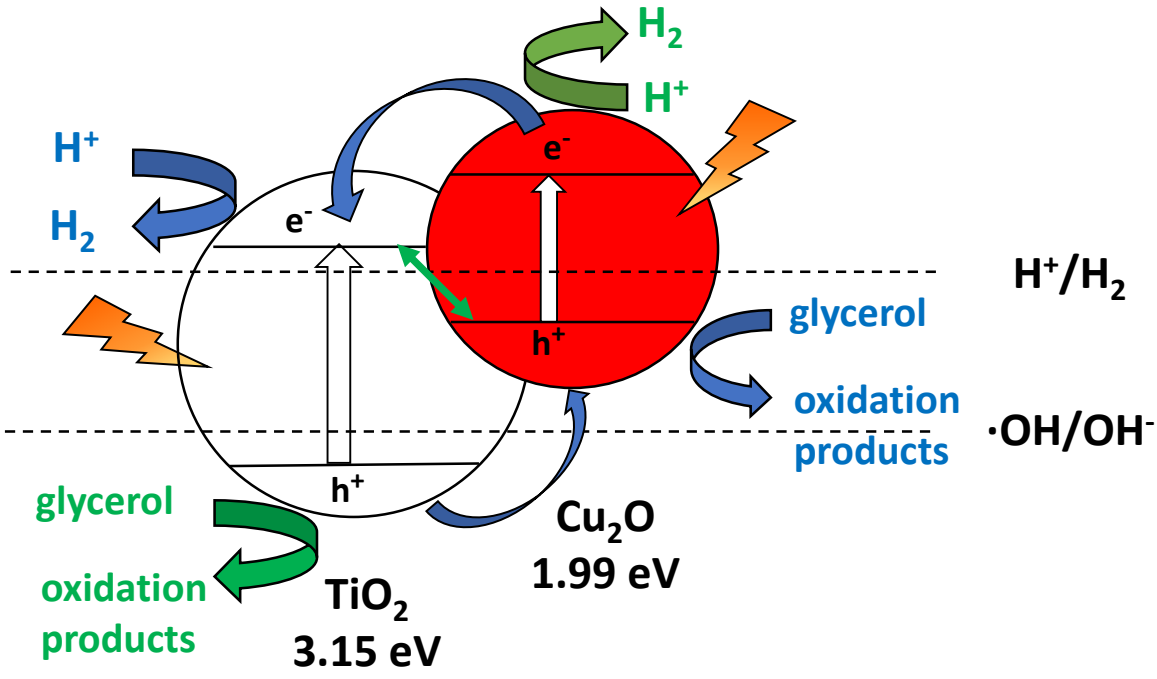

Figure 8. Energetic levels and possible charges transfer mechanism.

4. Conclusions

This work presents a facile way to prepare noble metal free photocatalysts for anaerobic heterogeneous solar/UV light reforming of glycerol in aqueous media using commercial TiO_2. Different amount of Cu_2O or 3% CuO were loaded on TiO_2 using ball milling and runs were carried out monitoring the glycerol conversion and the amount of hydrogen and CO_2 formed in the gas phase and that of 1,3-dihydroxyacetone and glyceraldehyde in the liquid phase. The results were compared with those of runs carried out using TiO_2 loaded with

platinum and/or coupled with copper oxide with the aim to verify the effectiveness of Cu_2O in replacing Pt.

3%wt Cu_2O – TiO_2 showed the best results, with glycerol conversion of ~ 33%, selectivity of 10.3% and 5.4% for DHA and GA respectively, CO_2 concentration of 0.16 mM, H_2 of 1.01 mM, corresponding to 0.17 mmol h^{-1} g^{-1}. These values are comparable with the ones obtained using Pt – TiO_2 except for GA, where Pt – TiO_2 showed no selectivity.

Photocatalysts characterized through X-Ray diffractions, Raman, UV–Vis spectroscopy, Specific Surface Area, Scanning electron microscopy/EDX and Photocurrent spectroscopy confirmed the formation of a heterostructure between TiO_2 and copper oxide and the effectiveness of platinum photodeposition and copper oxide – TiO_2 ball milling.

Declaration of Competing Interest

The authors declare that they have no known competing financial interests or personal relationships that could have appeared to influence the work reported in this paper.

Acknowledgements

This research did not receive any specific grant from funding agencies in the public, commercial, or not-for-profit sectors.

References

[1] V. Maslova, A. Fasolini, M. Offidani, S. Albonetti, F. Basile, Catal Today 380 (2021) 147–55. 10.1016/j.cattod.2021.03.008.

[2] A. González-Garay, N. mac Dowell, N. Shah, Discover Chemical Engineering 1(1) (2021) 2. 10.1007/s43938-021-00002-x.

[3] S. Gisbertz, B. Pieber, ChemPhotoChem 4(7) (2020) 456–75. 10.1002/cptc.202000014.

[4] M. Bellardita, S. Yurdakal, B.S. Tek, Ç. Değirmenci, G. Palmisano, V. Loddo, L. Palmisano, J. Soria, J. Sanz, V. Augugliaro, J Environ Chem Eng 9(4) (2021) 105308. 10.1016/j.jece.2021.105308.

[5] T. Gupta, R.P. Chauhan, J Environ Chem Eng 9(6) (2021) 106734. 10.1016/j.jece.2021.106734.

[6] Y. Zhao, Y. Li, L. Sun, Chemosphere 276 (2021) 130201. 10.1016/j.chemosphere.2021.130201.

[7] K. Maeda, K. Domen, J Phys Chem Lett 1(18) (2010) 2655–61. 10.1021/jz1007966.

[8] D. Zhao, Y. Wang, C.-L. Dong, Y.-C. Huang, J. Chen, F. Xue, S. Shen, L. Guo, Nat Energy 6(4) (2021) 388–97. 10.1038/s41560-021-00795-9.

[9] C.Y. Toe, C. Tsounis, J. Zhang, H. Masood, D. Gunawan, J. Scott, R. Amal, Energy Environ Sci 14(3) (2021) 1140–75. 10.1039/D0EE03116J.

[10] Y.-H. Chung, K. Han, C.-Y. Lin, D. O'Neill, G. Mul, B. Mei, C.-M. Yang, Catal Today 356 (2020) 95–100. 10.1016/j.cattod.2019.07.042.

[11] S. Çetinkaya, G. Khamidov, L. Özcan, L. Palmisano, S. Yurdakal, Front Chem 10 (2022). 10.3389/fchem.2022.856947.

[12] J. Corredor, M.J. Rivero, C.M. Rangel, F. Gloaguen, I. Ortiz, Journal of Chemical Technology & Biotechnology 94(10) (2019) 3049–63. 10.1002/jctb.6123.

[13] Q. Guo, Z. Ma, C. Zhou, Z. Ren, X. Yang, Chem Rev 119(20) (2019) 11020–41. 10.1021/acs.chemrev.9b00226.

[14] V. Kumaravel, S. Mathew, J. Bartlett, S.C. Pillai, Appl Catal B 244 (2019) 1021–64. 10.1016/j.apcatb.2018.11.080.

[15] M. Bellardita, E.I. García-López, G. Marcì, G. Nasillo, L. Palmisano, Eur J Inorg Chem 2018(41) (2018) 4522–32. 10.1002/EJIC.201800663.

[16] Y.H. Chung, K. Han, C.Y. Lin, D. O'Neill, G. Mul, B. Mei, C.M. Yang, Catal Today (2020) 95–100. 10.1016/j.cattod.2019.07.042.

[17] K.K. Mandari, J.Y. Do, S.V.P. Vattikuti, A.K.R. Police, M. Kang, J Alloys Compd 750 (2018) 292–303. 10.1016/j.jallcom.2018.03.294.

[18] N.S. Gultom, H. Abdullah, D.H. Kuo, Int J Hydrogen Energy 42(41) (2017) 25891–902. 10.1016/j.ijhydene.2017.08.198.

[19] S. ichiro Fujita,,H. Kawamori, D. Honda, H. Yoshida, M. Arai, Appl Catal B 181 (2016) 818–24. 10.1016/j.apcatb.2015.08.048.

[20] E. Wierzbicka, M. Altomare, M. Wu, N. Liu, T. Yokosawa, D. Fehn, S. Qin, K. Meyer, T. Unruh, E. Spiecker, L. Palmisano, M. Bellardita, J. Will, P. Schmuki, J Mater Chem A Mater 9(2) (2021) 1168–79. 10.1039/d0ta09066b.

[21] M. Muscetta, S. al Jitan, G. Palmisano, R. Andreozzi, R. Marotta, S. Cimino, I. di Somma, J Environ Chem Eng 10(3) (2022) 107735. 10.1016/j.jece.2022.107735.

[22] K.K. Mandari, J.Y. Do, S.V.P. Vattikuti, A.K.R. Police, M. Kang, J Alloys Compd 750 (2018) 292–303. 10.1016/j.jallcom.2018.03.294.

[23] A.M. Mohammed, S.S. Mohtar, F. Aziz, S.A. Mhamad, M. Aziz, J Environ Chem Eng 9(2) (2021). 10.1016/j.jece.2021.105138.

[24] M. Muscetta, R. Andreozzi, L. Clarizia, I. di Somma, R. Marotta, Int J Hydrogen Energy (2020) 28531–52. 10.1016/j.ijhydene.2020.07.225.

[25] K. Yang, G. Cheng, R. Chen, K. Zhao, Y. Liang, W. Li, C. Han, Energy Technology 10(1) (2022). 10.1002/ente.202100259.

[26] M. Bellardita, D. Virtù, F. di Franco, V. Loddo, L. Palmisano, M. Santamaria, Chemical Engineering Journal 431 (2022). 10.1016/j.cej.2021.134131.

[27] D. Reyes-Coronado, G. Rodríguez-Gattorno, M.E. Espinosa-Pesqueira, C. Cab, R. de Coss, G. Oskam, Nanotechnology 19(14) (2008) 145605. 10.1088/0957-4484/19/14/145605.

[28] J. Zhu, Z. Deng, F. Chen, J. Zhang, H. Chen, M. Anpo, J. Huang, L. Zhang, Appl Catal B 62(3–4) (2006) 329–35. 10.1016/j.apcatb.2005.08.013.

[29] R. Fiorenza, M. Bellardita, S. Scirè, L. Palmisano, Molecular Catalysis 455 (2018) 108–20. 10.1016/j.mcat.2018.06.002.

[30] C.-M. Wang, C.-Y. Wang, (2014). 10.1117/1.

[31] K. Phiwdang, S. Suphankij, W. Mekprasart, W. Pecharapa, Energy Procedia 34 (2013) 740–5. 10.1016/j.egypro.2013.06.808.

[32] Md.J. Nine, B. Munkhbayar, M.Sq. Rahman, H. Chung, H. Jeong, Mater Chem Phys 141(2–3) (2013) 636–42. 10.1016/j.matchemphys.2013.05.032.

[33] U. Balachandran, N.G. Eror, J Solid State Chem 42(3) (1982) 276–82. 10.1016/0022-4596(82)90006-8.

[34] J.L. Chen, M.M. Liu, S.Y. Xie, L.J. Yue, F.L. Gong, K.M. Chai, Y.H. Zhang, J Mol Struct 1247 (2022). 10.1016/j.molstruc.2021.131294.

[35] R. Fiorenza, M. Bellardita, S. Scirè, L. Palmisano, Catal Today (2019) 113–9. 10.1016/j.cattod.2017.12.011.

[36] J. Yu, Y. Hai, M. Jaroniec, J Colloid Interface Sci 357(1) (2011) 223–8. 10.1016/j.jcis.2011.01.101.

[37] J. Bandara, C.P.K. Udawatta, C.S.K. Rajapakse, Photochemical and Photobiological Sciences 4(11) (2005) 857–61. 10.1039/b507816d.

[38] Y.H. Zhang, M.M. Liu, J.L. Chen, K.F. Xie, S.M. Fang, Journal of Physics and Chemistry of Solids 152 (2021). 10.1016/j.jpcs.2021.109948.

[39] M. Tavakolian, K. Keshavarz, M. Hosseini-Sarvari, Molecular Catalysis 514 (2021). 10.1016/j.mcat.2021.111810.

[40] S. Lv, Y. Wang, Y. Zhou, Q. Liu, C. Song, D. Wang, J Alloys Compd 868 (2021). 10.1016/j.jallcom.2021.159144.

[41] J. Duan, H. Zhao, Z. Zhang, W. Wang, Ceram Int 44(18) (2018) 22748–59. 10.1016/j.ceramint.2018.09.062.

[42] M.E. Aguirre, R. Zhou, A.J. Eugene, M.I. Guzman, M.A. Grela, Appl Catal B 217 (2017) 485–93. 10.1016/j.apcatb.2017.05.058.